The 1.25 Å Resolution Structure of the Diheme NapB Subunit of Soluble Nitrate Reductase Reveals a Novel Cytochrome *c* Fold with a Stacked Heme Arrangement[†,‡]

Ann Brigé,[§,||] David Leys,[§,||] Terrance E. Meyer,[⊥] Michael A. Cusanovich,[⊥] and Jozef J. Van Beeumen*[,§]

Laboratory of Protein Biochemistry and Protein Engineering, State University of Gent, Ledeganckstraat 35, B-9000 Gent, Belgium, and Department of Biochemistry, University of Arizona, Tucson, Arizona 85721

Received December 11, 2001; Revised Manuscript Received February 7, 2002

ABSTRACT: The diheme cytochrome NapB constitutes the small subunit of a periplasmic nitrate reductase found in a wide variety of bacterial species, including pathogens. The NapB protein is essential in transferring electrons to the large catalytic subunit NapA, which subsequently reduces nitrate to nitrite. Here we present the crystal structure of a proteolyzed form of recombinant NapB from *Haemophilus influenzae*, which was determined by the multiple-wavelength anomalous dispersion (MAD) method at 1.25 Å resolution. This structure shows an unprecedented fold, confirming that NapB proteins belong to a new class of cytochromes. The two heme groups have nearly parallel heme planes and are stacked at van der Waals distances with an iron-to-iron distance of only 9.9 Å, two structural features that are also present in the split-Soret diheme cytochrome *c* from *Desulfovibrio desulfuricans* ATCC 27774, which is otherwise unrelated in the peptide chain folding pattern. The two propionate side chains on both heme groups are hydrogen-bonded to each other, a structural characteristic that to date also has not been reported in any other heme protein. The propionates of one of the heme groups are pulled toward the interior of the molecule due to a salt bridge and a number of hydrogen bonds between the propionates and conserved residues. We propose a hypothetical but plausible model of the NapAB complex in which the four redox centers are positioned in a virtually linear configuration which spans a distance of nearly 40 Å, suggesting an efficient pathway for the transfer of electrons from NapC, the physiological electron donor of NapB, to a nitrate molecule at the catalytic site of NapA.

Periplasmic nitrate reductases (Naps)[1] constitute one of the three types of bacterial nitrate reductases (reviewed in ref *1*). At least four Nap proteins are involved in the periplasmic reduction of nitrate to nitrite. NapA is the large catalytic subunit of this heterodimeric reductase and contains a [4Fe-4S] cluster in addition to a bis-molybdopterin guanine dinucleotide (MGD) cofactor. The small subunit of the enzyme is a diheme cytochrome *c* (NapB) that is involved in the transfer of electrons to NapA, which subsequently reduces nitrate to nitrite. The subunits are thought to interact in a hydrophobic manner (*2*). The membrane-anchored tetraheme cytochrome *c* NapC is the direct electron donor to NapB and receives electrons from oxidation of the quinol pool in the cytoplasmic membrane. Finally, NapD plays a role in the maturation of NapA (*3*). Within the various bacterial species that exhibit Nap activity, up to three out of five other Nap proteins can be found in different combinations with NapDABC. NapE and NapK are small integral membrane proteins with unknown function. NapK has so far only been identified in *Rhodobacter sphaeroides* (*4, 5*). The function of the iron−sulfur proteins NapFGH, of which all three structural genes are found in *Escherichia coli* and *Haemophilus influenzae*, is also unclear. Mutational analysis of the *E. coli* NapFGH proteins has shown that none of them is essential for electron transfer to NapA (*6*). It has been proposed that the NapGH complex constitutes a quinol oxidase that enables direct electron transport to NapB (*3*). In this respect, it is interesting to mention that, in *Shewanella putrefaciens*, the *napGH* genes are part of the *nap* cluster but that the *napC* gene is independently transcribed and is called *cymA*. Other functions, such as facilitating electron flow to the NapAB complex (NapF), the assembly or processing of the iron−sulfur cluster of NapA (NapF), or being a redox sensor (NapH) coupled to the control of electron flow, have been suggested for the iron−sulfur proteins (*3, 5*).

[†]J.J.V.B. is indebted to the Bijzonder Onderzoeksfonds (State University of Gent) for Project 12050198 and to the Fund for Scientific Research for Project G.0054.97. D.L. is a postdoctoral researcher of the FWO-Flanders. T.E.M. and M.A.C. were supported by a grant from the National Institutes of Health (GM 21277).

[‡] Atomic coordinates have been deposited with the Research Collaboratory for Structural Bioinformatics (RCSB) Protein Data Bank (entry 1JNI).

* To whom correspondence should be addressed: Laboratory of Protein Biochemistry and Protein Engineering, K. L. Ledeganckstraat 35, B-9000 Gent, Belgium. Telephone: +32-(0)9-264-51-09. Fax: +32-(0)9-264-53-38. E-mail: jozef.vanbeeumen@rug.ac.be.

[§] State University of Gent.

[||] Both authors contributed equally to this work.

[⊥] University of Arizona.

[1] Abbreviations: EPR, electron paramagnetic resonance; EXAFS, extended X-ray absorption fine structure; FAD, flavin adenine mononucleotide; FCSD, flavocytochrome *c* sulfide dehydrogenase; FOM, figure of merit; MAD, multiple-wavelength anomalous dispersion; MCD, magnetic circular dichroism; MGD, molybdopterin guanine dinucleotide; Nap, periplasmic nitrate reductase; SSC, split-Soret cytochrome *c*; V_M, Matthews coefficient (cubic angstroms per dalton).

10.1021/bi012144b CCC: $22.00
Published on Web 03/22/2002

Since the number of bacterial species in which *nap* genes are identified is still increasing, periplasmic nitrate reduction is more widespread than originally assumed. Moreover, since these genes are present in all major groups of prokaryotes (for an overview, see ref *1*), periplasmic nitrate reductases appear to be ubiquitous in nature. Nap activity is therefore believed to make a significant contribution to the global nitrogen cycle. Remarkably, there are some differences in *nap* gene expression within various organisms. Also, the role of Nap activity seems to vary between the different bacterial species or even in the same organism under different metabolic conditions. In several species, including *Rhodobacter capsulatus*, *R. sphaeroides*, and *Paracoccus pantotrophus*, Nap activity is used for cellular redox balancing by which nitrate is used as a preferred electron sink to dissipate excess reducing power that is generated, for instance, during growth on highly reduced carbon substrates (*2*, *7*, *8*). Periplasmic nitrate reduction can also be the first step in denitrification performed by organisms such as *P. pantotrophus* and *R. sphaeroides* f. sp. *denitrificans* (*9*−*11*). In *Ralstonia eutropha*, Nap is involved in the adaptation to anaerobic growth (*12*). In *E. coli* and *H. influenzae*, two species found in the human body where the concentration of nitrate is very low, Nap is suggested to fulfill a nitrate scavenging role (*13*, *14*). Besides their presence in *H. influenzae*, *nap* genes have also been found more recently in a number of other pathogenic bacteria, including *Pasteurella multocida* (*15*), *Vibrio cholerae* (*16*), *Campylobacter jejuni* (*17*), *Legionella pneumophila* (http://genome3.cpmc.columbia.edu), *Salmonella typhimurium* (http://genome.wustl.edu/gsc/Projects/bacteria.shtml), and *Yersinia pestis* (http://www.sanger.ac.uk). Despite their occurrence in a phylogenetically diverse range of bacteria and their involvement in important and versatile metabolic processes, few Nap proteins have been characterized. The soluble domain of the NapC protein from *P. pantotrophus* has been studied spectroscopically and electrochemically (*18*). The molybdenum center of the Nap enzyme from the same organism was studied using EPR and EXAFS (*19*), and models of the catalytic cycle of this enzyme have been presented (*20*). Recently, the NapAB complex from *P. pantotrophus* has been studied by MCD and EPR, indicating that both hemes in NapB are low-spin and have two histidines as axial ligands (*21*). Except for the crystal structure of a NapA homologue identified in *Desulfovibrio desulfuricans* ATCC 27774 (*22*), no structural information about Nap proteins is available. The *Desulfovibrio* protein is folded into four domains that are all involved in binding of the bis-MGD cofactor, which is deeply buried in the interior of the molecule. The molybdenum active site is accessible from the surface through a funnel-like cavity, a structural feature common to all molybdopterin-containing enzymes, and is positioned 12 Å from the [4Fe-4S] cofactor. It has been proposed that for redox centers placed within a maximal distance of 14 Å, the electron transfer rate is faster than the average rate of catalysis at the enzymatic site, regardless the nature of the intervening protein medium. This single characteristic feature has been selected in the course of evolution to allow efficient electron transfer and directional specificity (*23*).

The amino acid sequences of NapB cytochromes show no significant similarity with any other cytochrome *c*. Furthermore, the positioning of the two heme-binding sites in NapB is unprecedented: the N-terminal heme-binding site is located nearly halfway along the protein sequence and is separated from the second heme-binding site by at most 35 residues (*5*, *12*, *24*−*26*). These characteristics suggest that NapB proteins belong to a new class of cytochrome *c*.

The crystal structures of four diheme cytochromes have been reported so far. The cytochrome c_4 from *Pseudomonas stutzeri* (*27*), the cytochrome subunit of the flavocytochrome *c* sulfide dehydrogenase (FCSD) from *Chromatium vinosum* (*28*), and cytochrome *c* peroxidase (CCP) from *Pseudomonas aeruginosa* (*29*) are all related to class I monoheme cytochromes *c*. A preliminary model is available of the structure of the fourth protein, namely, the split-Soret cytochrome *c* (SSC) from *D. desulfuricans* ATCC 27774 (*30*). Within these proteins, the angle between the two heme planes varies considerably while, on the other hand, the distances between the iron atoms are relatively similar and lie between 16 and 21 Å. SSC is the only exception, in which the distance between the two irons is only 9 Å. The two hemes in this diheme cytochrome are stacked in a unique manner, with their edges overlapping at van der Waals distance. The SSC is also unusual in that the two identical subunits fold to create a single heme binding domain.

Here we report the first structural data for a NapB protein obtained by the multiple-wavelength anomalous dispersion method (MAD) as the source of phasing information. The structural organization of the two heme groups shows a resemblance to the stacked heme arrangement in SSC, whereas the overall fold of the two proteins is dissimilar.

EXPERIMENTAL PROCEDURES

Crystallization. Crystals of recombinant NapB were obtained as described elsewhere (*31*) by the hanging-drop vapor diffusion method, using 1.75 M ammonium sulfate at pH 5.5 as a precipitant. The tetragonal crystals belong to space group $P42_12$ with the following unit cell dimensions: $a = b = 78.6$ Å, $c = 29.0$ Å, and $\alpha = \beta = \gamma = 90°$. If the molecular mass of the mature protein (14 748 Da) and one molecule in the asymmetric unit are taken into account, the solvent content was calculated to be only 16.5%, an unusually low value for macromolecular crystals. However, analyses of the dissolved crystals by electrospray ionization mass spectrometry and N-terminal amino acid sequence analysis clearly indicated that proteolysis had occurred at both the N- and C-termini of the recombinant protein. Consequently, assuming the molecular mass of the crystallized form of NapB to be 8500 Da, we estimated the solvent content to be 53%. Therefore, the volume per unit of molecular weight (V_M) equaled 2.64 Å^3/Da (*32*). These values are within the normal range observed for protein crystals.

Data Collection and Processing. A native data set of a flash-frozen crystal was collected at synchrotron beamline X11 ($\lambda_1 = 0.9073$ Å) at DORIS (HASYLAB, DESY, Hamburg, Germany) up to 1.8 Å resolution, using a MAR-CCD imaging-plate detector (Table 1). The same crystal was used to collect the X-ray diffraction data for MAD phasing at beamline X31 at DORIS, on a MAR-Research imaging-plate detector. Prior to the data collection, an X-ray fluorescence spectrum was recorded in the vicinity of the Fe−K absorption edge. Interpretation of the spectrum resulted in the real (f') and imaginary (f'') terms of the

Table 1: Summary of the Crystallographic Data Statistics

Diffraction Data				
	λ_1	λ_2	λ_3	λ_4
wavelength (Å)	0.9280	1.7384	1.7352	0.9640
resolution limit (Å)	40.0−1.8 (1.83−1.8)[a]	15.0−2.5 (2.6−2.5)	15.0−2.3 (2.38−2.30)	10.0−1.25 (1.26−1.25)
no. of measured reflections	77077	65932	33142	214619
no. of unique reflections	16375	3329	4172	22337
completeness (%)	94.5 (93.3)	99.8 (100)	98.6 (98.1)	84.4 (65.47)
$I/\sigma(I)$	35.49 (12.76)	22.30 (7.92)	11.24 (3.3)	17.0 (1.37)
R_{merge}[b] (%)	2.7 (8.7)	9.8 (24.2)	11.4 (29.2)	8.9 (31.6)

Phasing Statistics			
	λ_1[c]	λ_2	λ_3
R_{cullis}[d]			
centric	/	0.51	0.69
acentric	/	0.52	0.68
anomalous	0.78	0.85	0.78
phasing power[e]			
centric	/	1.76	1.11
acentric	/	2.42	1.49
figure of merit (15−2.3 Å)	0.63		

Refinement Statistics	
resolution range (Å)	10.0−1.25
no. of independent reflections	20831
no. of non-hydrogen atoms	688 (1126 with hydrogens)
no. of protein residues	64
no. of water molecules	129
crystallographic *R* factor	0.1596
R_{free}	0.2165
bond length deviation (Å)	0.013
bond angle deviation (deg)	2.5
average temperature factor (Å^2)	
for all non-hydrogen atoms	26.86
for protein main chain atoms	20.87
for protein side chain and solvent atoms	30.30
for cofactor atoms	18.53
for solvent molecules	48.60

[a] Numbers in parentheses refer to the values for the outer resolution shell. [b] $R_{merge}(I) = \sum_h\sum_i|I_{h,i} - \langle I_h\rangle|/\sum_h\sum_i I_{h,i}$, where I is the observed intensity, i represents the replicate measurements of a given reflection h, and $\langle I\rangle$ is the average intensity of multiple observations of symmetry-related reflections. [c] λ_1 was used as the reference wavelength for phasing purposes. [d] $R_{cullis} = \sum[|F_H| - (|F_{PH}| - |F_P|)/\sum(|F_{PH}| - |F_P|)]$, where F_H represents the calculated heavy atom structure factor. [e] Phasing power $= \langle|F_{H(calc)}|/|E|\rangle$, where $F_{H(calc)}$ is the calculated anomalous difference and E is the lack of closure.

anomalous scattering factor, as a function of photon energy. The expression for conversion of X-ray wavelength and X-ray energy ($E = 12398.38/\lambda$) was applied to determine the corresponding wavelengths. Subsequently, diffraction data were collected at the two different wavelengths [$\lambda_2 =$ 1.7384 Å (7131 eV, point of inflection) and $\lambda_3 = 1.7353$ Å (7145 eV, peak)] which correspond to the minimum f' and maximum f'' values, respectively. At wavelength λ_2, a total of 180° of data were collected to 99.8% completeness, using 1° oscillation per frame; 83° of data were collected at λ_3 to 98.6% completeness. The native data set collected at λ_1 was used for scaling purposes; λ_1 was also chosen as the remote wavelength. High-resolution data at a fourth wavelength (λ_4 = 0.9640 Å) were used for refinement. This fourth data set was collected at ESRF (Grenoble, France) on microfocus beamline ID13 (*33*).

The measured intensities were integrated and scaled with DENZO/SCALEPACK (*34*), resulting in one data set for each wavelength. Although the crystal diffracted to 1.1 Å at λ_4, the data processing statistics were only significant up to 1.25 Å. The CCP4 program package was used to merge the scaled data of $\lambda_1-\lambda_3$, to convert the intensities to structure factors, and to scale together the different wavelength data relative to λ_1, using the programs FHSCAL and SCALEIT (*35*).

Extraction of Phase Information from the MAD Data. The anomalous difference Patterson map calculated from the λ_3 data showed two clear peaks from which the position of one of the two expected Fe sites could be determined. The second Fe site was found by difference Fourier synthesis using the phase information from the first determined site.

The calculation of the MAD phases and refinement of the positions of the two iron atoms were carried out with all diffraction data of $\lambda_1-\lambda_3$ up to 2.3 Å. The occupancy and the position of the two sites were refined using MLPHARE (*36*), converging to an overall figure of merit (FOM) of 0.63 for the resolution range of 15−2.3 Å.

Model Building and Refinement. Using the obtained MAD phases, the electron density map was calculated with FFT from the CCP4 suite of programs (*35*). The software package TURBO-FRODO (*37*) was used for graphical interpretation of the electron density map. The initial experimental map (Figure 1a) was improved by density modification using DM from the CCP4 package (*35*), and included solvent flattening and histogram matching. The resultant map proved to be of good quality; the density of nearly all amino acid side chains

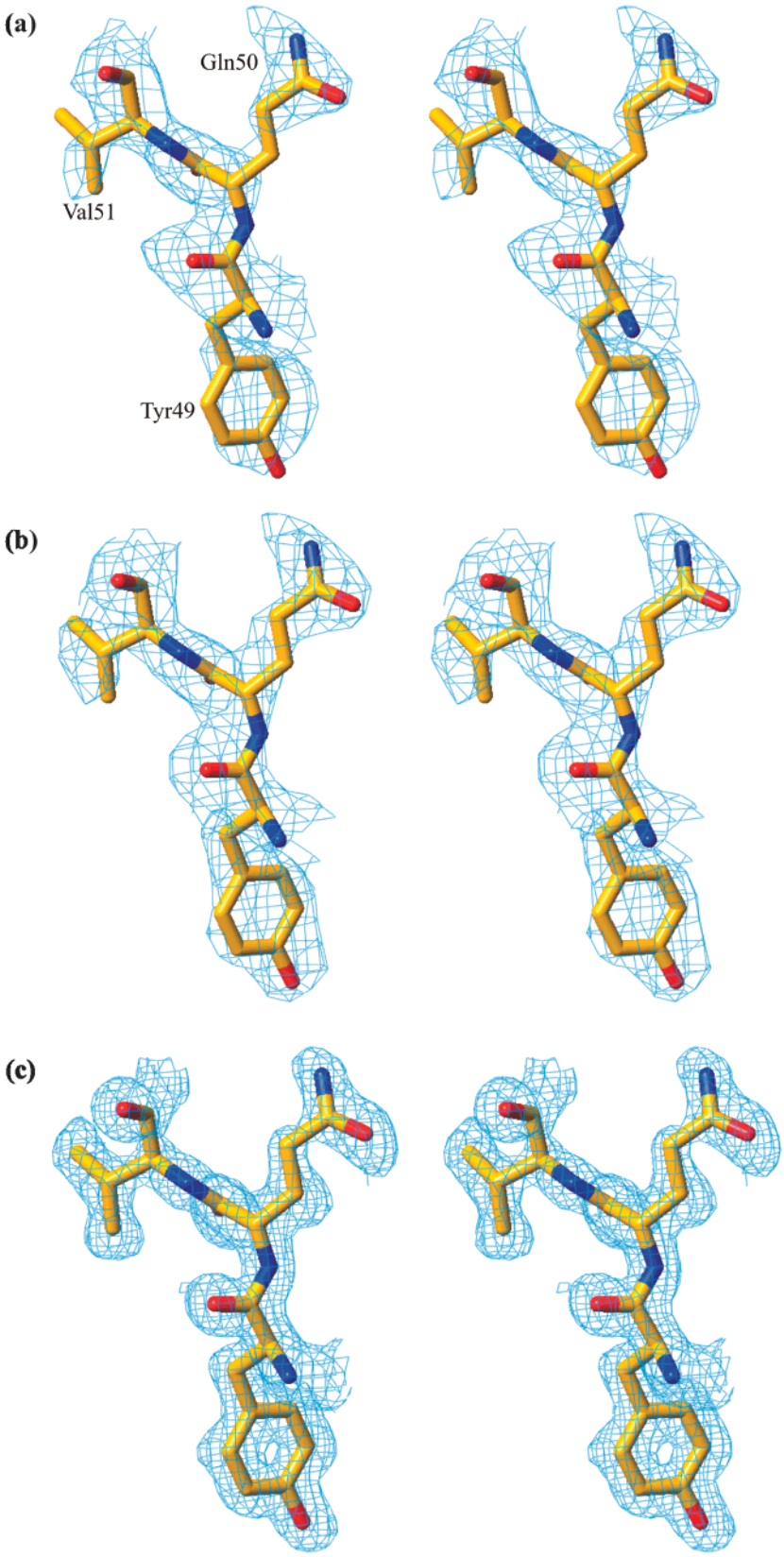

FIGURE 1: Stereoview of a section of the electron density map to demonstrate its improvement in the course of the refinement process. The maps were contoured at 1σ with the final model (Tyr49-Gln50-Val51) superposed. The final model is colored according to atom type with oxygen atoms in red and nitrogen atoms in blue. (a) Map calculated solely with MAD phasing information at 2.3 Å obtained from MLPHARE (*36*). (b) Map calculated using the phases obtained after density modification with the program DM (*35*). (c) Map after several cycles of REFMAC (*39*) and with high-resolution data up to 1.24 Å. The maps were drawn using TURBO-FRODO (*37*).

was well-defined (Figure 1b), and even water molecules could already be distinguished.

The program *ARP/wARP* 5.0 (*38*), which contains an autotracing module, was used to successfully trace the

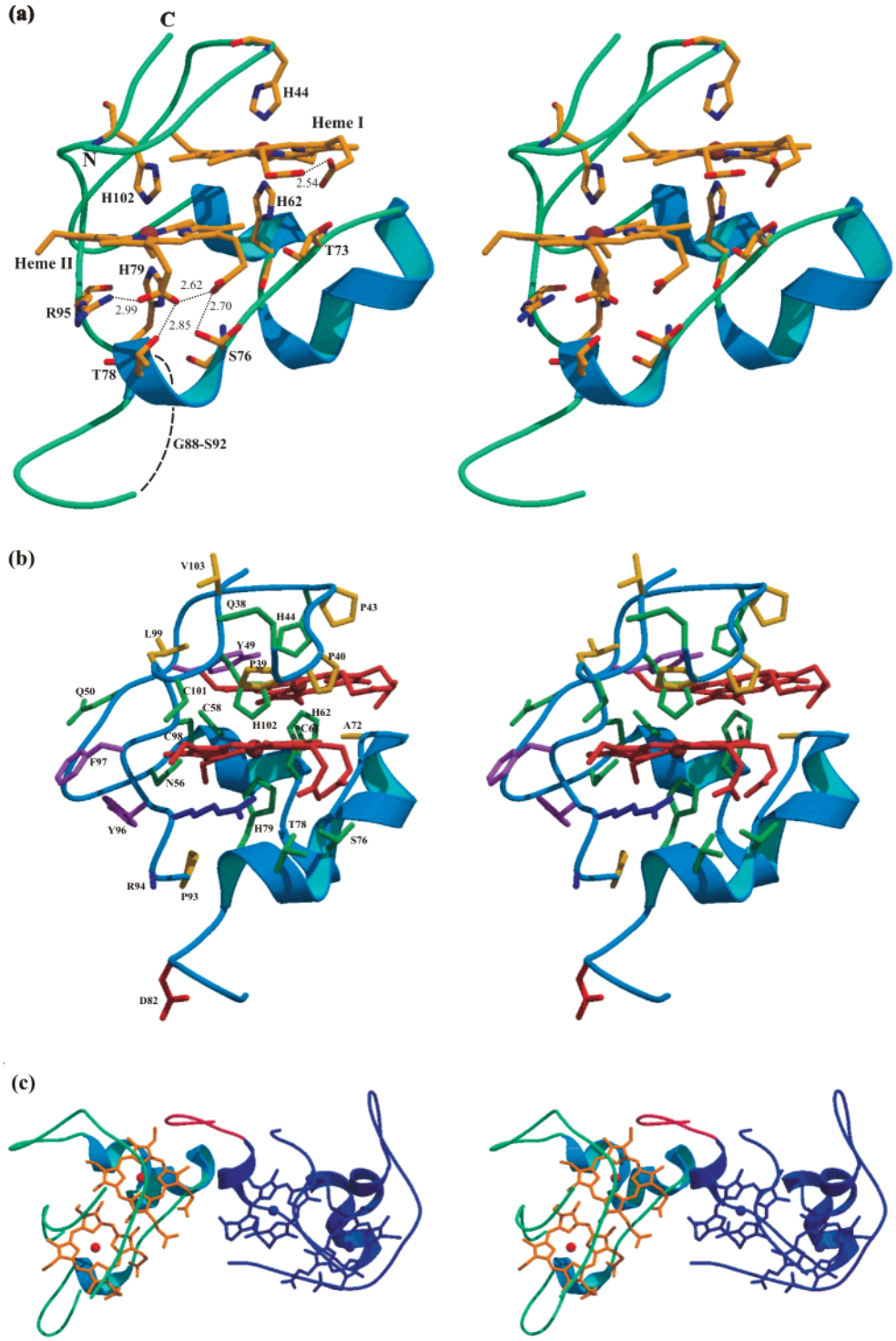

FIGURE 2: (a) Stereoimage of the overall fold of NapB and of the arrangement of the two heme groups. The two heme groups with their histidine ligands and conserved residues Thr73, Ser76, Thr78, and Arg95 are shown in ball-and-stick representation. The N-terminal and C-terminal ends are denoted as N and C, respectively. The missing stretch of Gly88−Ser92 is denoted as a thick dashed line. The salt bridge and hydrogen bonds are shown as a thin dashed line together with the average bond lengths. (b) Ribbon diagram of NapB with the conserved residues drawn in colored sticks, according to the following code: green for polar, yellow for apolar, purple for aromatic, red for negatively charged, and blue for positively charged. The figure is rotated 30° counterclockwise along the vertical axis relative to the orientation in panel a. (c) Image illustrating the characteristic packing of two NapB molecules within the crystal. The protruding stretch is shown in red. The orientation of the molecule at the left in panel c is rotated 90° clockwise along the horizontal axis and 45° counterclockwise along the vertical axis with respect to the view in panel a. All figures were generated using Molscript (*42*) and Raster3D (*43*).

polypeptide chain and model most of the amino acid side chains. The model was refined using the maximum likelihood-based program REFMAC (*39*) and using all diffraction data up to 1.25 Å resolution. Refinement proceeded with cycles of positional and individual *B*-factor refinement alternating with model building, using visual inspection of the maps and the program TURBO-FRODO (*37*). The *R* factor decreased from 27.0 to 22.1% after water molecules were added to the model by solvent building *ARP/wARP* 5.0 (*38*) (Figure 1c). Refinement was completed with the

program SHELXL-97 (*40*) introducing anisotropic refinement of the *B* factors and including "riding" hydrogen atoms. The final model has an *R* of 0.16 and an R_{free} of 0.22; it consists of residues 38−87 and 93−105, two heme groups, and 129 water molecules. In addition to the amino acid stretches at the N- and C-termini, residues 88−92 and some of the side chains were not visible in the electron density, and were therefore omitted from the model. The refinement statistics for the final model are summarized in Table 1.

RESULTS AND DISCUSSION

Protein Fold. The crystallized form of NapB has an elongated shape with approximate dimensions of 25 Å × 25 Å × 34 Å. The polypeptide chain is folded into three short α-helices (Gln57−His62, Asn66−Ser70, and Pro77−His79) that are connected by large loops (Figure 2a). The polypeptide chain is wrapped around the two heme groups that are situated on one side of the molecule with the propionate side chains oriented toward the solvent. Nearly all of the residues that are conserved among the NapB family either are lining the heme pockets or are found in the vicinity of the heme groups (Figure 2b). Thus, most of the missing amino acids at the N-terminus and C-terminus are not likely to be essential for the function of NapB in electron transfer but may be necessary for docking to the electron donor NapC or to the electron acceptor NapA.

A search in the Protein Data Base using the EMBL Dali server (*41*) did not show significant similarity to any previously determined protein fold. Therefore, we suggest that the three-dimensional structure of NapB constitutes a novel cytochrome fold. This is consistent with the absence of sequence similarity between NapB and any other protein, and with the unprecedented positioning of the two heme-binding sites and axial ligands. A closer look at the relative orientations of the eight molecules per unit cell in the NapB crystal revealed that the Gly84 and Asp85 residues of each NapB molecule are closely packed to the edge of one of the heme groups of a neighboring molecule (Figure 2c). Therefore, we have to take into consideration the possibility that the protruding nature of the Met81−Val87 stretch might be a likely consequence of this tight packing.

Arrangement of the Two Heme Groups. The overall heme arrangement is also shown in Figure 2a. The two hemes are nearly stacked on one another and are in van der Waals contact. They are approximately related by a 2-fold rotation axis that is nearly parallel to the heme planes and perpendicular to the plane of the figure. The closest distance between atoms of the two roughly parallel heme planes is only 4 Å, while the distance between the irons in the heme pair is 9.9 Å. Closer packing of the two hemes is impossible because the methyl carbon on pyrrole ring C is in direct van der Waals contact with the histidine coordinating the adjoining heme.

On the basis of the electron density, it was confirmed that both heme groups are covalently bound to the polypeptide chain by cysteinyl thioether linkages, and that both hemes have histidine residues as axial ligands. The imidazole rings of the histidines are close to being coplanar for both the heme groups, and are arranged so that they make an angle of ∼90° with the heme planes. This configuration is a necessary consequence of the limited space in the two hydrophobic heme pockets. The sixth ligand of heme I, His44, is rigidly kept in its conformation by a hydrogen bond to the oxygen backbone atom of Ser45, while being tightly packed against the side chains of Val42 and Pro43. His79, the sixth ligand of heme II, is wedged between the side chains of Ile75 and Arg95 and does not appear to have a hydrogen bonding partner.

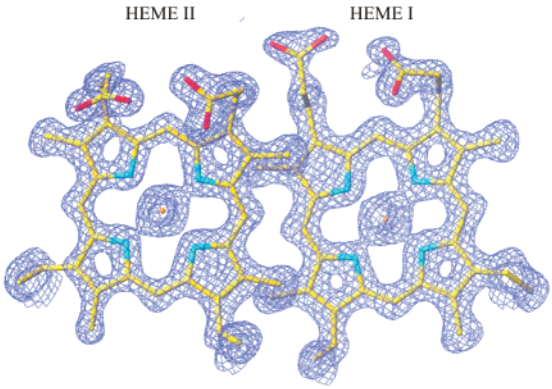

FIGURE 3: Image of the electron density for both heme groups, showing the orientation of the propionates. Shown is the sigmaA weighted $2F_o - F_c$ map, contoured at 2σ and superposed with the final model colored according to atom type.

One of the propionates of heme I is protruding into the solvent region, whereas the other propionate is slightly withdrawn from the solvent by a hydrogen bond with Thr73 (Figure 3). In contrast, both the propionates of heme II are pulled inward, which could be required for complex formation with either NapA or NapC. The heme propionates of the monoheme cytochrome b_5 from *Ectothiorhodospira vacuolata* (*44*) are also bent toward the interior of the molecule, which is accomplished by the formation of hydrogen bonds to a tyrosine and a serine. In addition, both propionates form salt bridges with a conserved lysine residue. In NapB, the propionates of heme II are restrained by a salt bridge between the propionate on ring D and the strictly conserved Arg95 (3.0 Å), and by a hydrogen bond between the same propionate and a conserved Ser/Thr78 (2.8 Å) (Figure 2a). Additionally, the propionate on ring C is hydrogen-bonded to the propionate on ring D (2.6 Å), as well as to the mostly conserved residue Ser76 (2.7 Å). In heme I, both propionates are also hydrogen-bonded to one another at a very short distance of 2.5 Å. There is also a hydrogen bond between the N backbone of Thr73 and the propionate on ring D. As far as we know, these are the first examples of hydrogen bond formation between the propionates of a single heme, which is therefore a structural novelty characteristic to NapB. However, it is possible that the interaction between the propionates is merely a result of the low pH in the crystallization conditions and may therefore not be maintained at physiological pH.

Conversely, hydrogen bonds between the propionates of two different hemes have been described previously, for instance, in the flavocytochrome *c* sulfide dehydrogenase of *C. vinosum* (*28*) and in the hydroxylamine oxidoreductase of *Nitrosomonas europaea* (*45*). In the latter cases, the heme groups are completely enclosed by the polypeptide chain. The propionate side chains have limited access to the solvent since they are buried in the protein core where the pK_a can shift significantly from the standard values. However, in the case of NapB, both propionates reside on the protein surface,

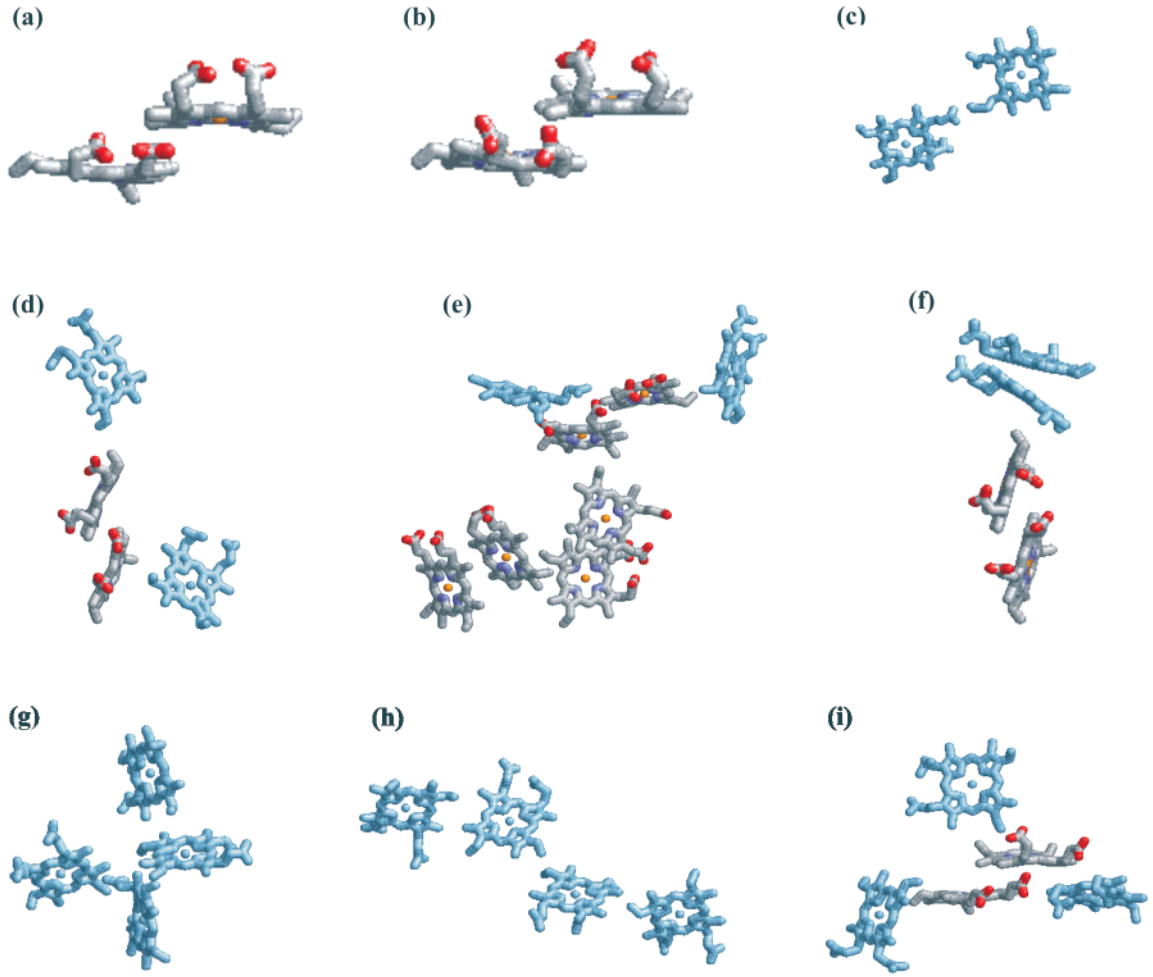

FIGURE 4: Heme arrangement of NapB (a; 1JNI) and SSC (b; 1DDC) compared to that of flavocytochrome *c* sulfide dehydrogenase from *C. vinosum* (c; 1FCD), flavocytochrome *c* fumarate reductase from *S. putrefaciens* (d; 1D4D), hydroxylamine oxidoreductase (e; 1FGJ), cytochrome c_{554} from *N. europaea* (f; 1BVB), cytochrome c_3 from *Desulfovibrio gigas* (g; 1WAD), the tetraheme cytochrome *c* of the photosynthetic reaction center of *Rhodopseudomonas viridis* (h; 5PRC), and cytochrome *c* nitrite reductase from *Sulfurospirillum deleyianum* (i; 1QDB). PDB file numbers are given in parentheses. The diheme pairs with a parallel stacked heme arrangement are colored according to atom type. The other diheme groups are shown in monochrome blue. The figures were generated using Rasmol (*46*).

indicating that even solvent-exposed hemes do not necessarily contribute fully to the negative charge.

Comparison with Other Diheme and Multiheme Cytochromes. There are some striking similarities between the heme arrangement in NapB and the split-Soret diheme cytochrome *c* from *D. desulfuricans* ATCC 27774 (*30*), although there is no relationship in peptide chain folding (Figure 4). Both cytochromes distinguish themselves from the other diheme cytochromes with known three-dimensional structure by much shorter iron-to-iron distances and by nearly parallel heme planes that are stacked within van der Waals distances. The distances separating the irons in the cytochrome c_4 from *Pseudomonas stutzeri* (*27*), the cytochrome subunit of the flavocytochrome *c* sulfide dehydrogenase (FSCD) from *C. vinosum* (*28*), and the cytochrome *c* peroxidase (CCP) from *Ps. aeruginosa* (*29*) all lie within the range of 16−21 Å. The heme planes are not parallel, but have inclination angles of 30° for the first two proteins, and of 90° for CCP. In none of the latter proteins are the protophorphyrin planes in van der Waals contact.

There are, however, two important differences between the heme organization in NapB and SSC. In the latter, the imidazole rings of the histidines ligating the iron of the inner heme are nearly perpendicular, whereas in NapB the histidines of both hemes are approximately coplanar. The second difference is that in the dimeric molecule SSC, the polypeptide chain of each monomer supplies the sixth axial histidine ligand to the heme of the other monomer, indicating that the dimer is the functional unit of SSC.

Although the heme organization in NapB and SSC differs substantially from that observed in the other diheme cytochromes, the characteristically short interiron distances are also found in multiheme cytochromes. The multiple hemes in these proteins can often be clustered into different diheme pairs, with a parallel, perpendicular, or "edge-on" type of diheme packing arrangement (*47*) (Figure 4). When we consider the multiheme cytochromes with stacked diheme pairs, hemes I and II of NapB and SSC can be superimposed on hemes I and III of the tetraheme cytochrome c_{554} from *N. europaea* (*47*), on the I/II, III/V, and VI/VII heme pairs from hydroxylamine oxidoreductase of *N. europaea* (*45*), on heme III and IV of the cytochrome *c* nitrite reductase from *Sulfurospirillum deleyianum* (*48*), and on hemes II and III of the soluble fumarate reductases from *Shewanella frigidimarina* (*49*, *50*) and *S. putrefaciens* (*51*). These diheme packing motifs all have interheme iron distances around 9.5 Å and have been suggested to represent favorable interactions

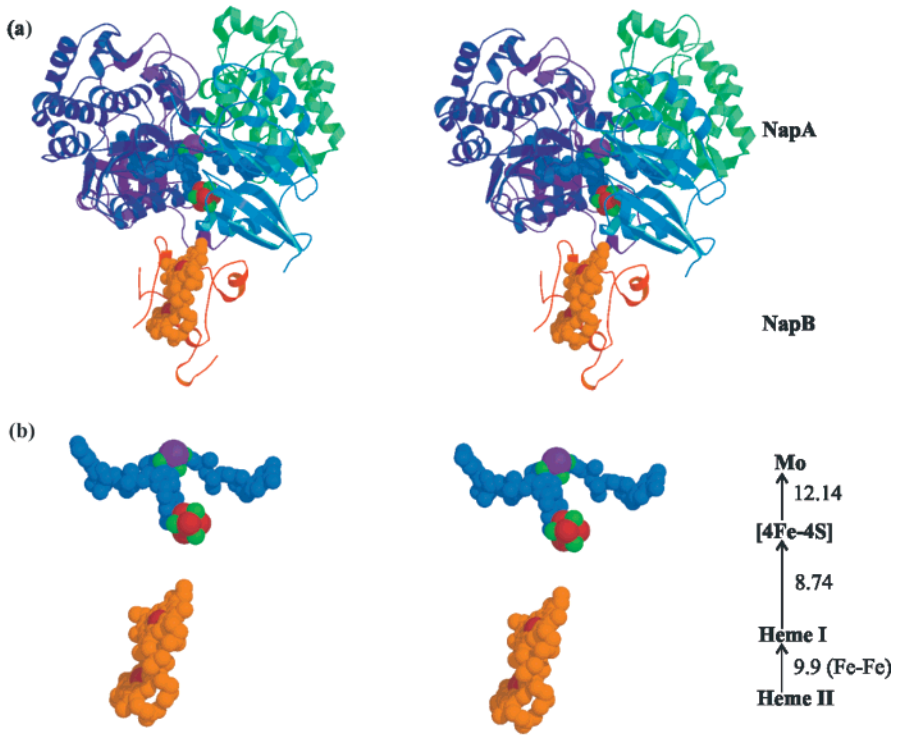

FIGURE 5: (a) Stereo representation of the hypothetical docking model between NapA and NapB. Both molecules are shown as a ribbon diagram, and the different prosthetic groups are shown in a space-filling representation. (b) Stereoview of the molecular wire of redox centers in the NapAB complex. The distances in angstroms between the different centers are indicated on the right. The figures were generated using Molscript (*42*) and Raster3D (*43*).

between hemes that facilitate electron transfer between them (*47*).

At present, all diheme and multiheme cytochromes exhibiting this type of heme packing have been isolated from organisms that either oxidize or reduce nitrogen- or sulfur-containing compounds as their primary energy source. The special arrangement of the heme centers seems to be of functional significance, but the reason these structural similarities are found in otherwise unrelated proteins remains unknown. We might speculate that the requirement to pack the relatively large and hydrophobic heme groups at distances of less than 14 Å has resulted in the evolutionary solution of packing these hemes in proximity, partially satisfying the need of protection from the solvent by mutual van der Waals interactions. There are, however, only a few possible orientations in which two heme groups that are both bis-histidine ligated and covalently bound to the CXXCH motif can pack together without steric hindrance. It is exactly these orientations that are observed in several multiheme cytochromes of unrelated evolutionary origin. We therefore suggest the apparent structural relationship of the heme core of these redox proteins to arise from the packing of these cofactors prior to folding of the respective polypeptide chains. The native conformation of the protein effectively selects one of the possible combinations of diheme packing motifs that can arise between the multiple hemes, resulting in similar heme arrangements for unrelated proteins.

NapAB Complex. In the NapA homologue of *D. desulfuricans*, the catalytic molybdenum site is coordinated by two MGD cofactors and is located at the bottom of a 15 Å deep funnel-like cavity (*22*). The latter is a feature common to other molybdopterin-containing enzymes and, in the case of NapA, ensures that a nitrate molecule can access the catalytic site. The electrons that are required for the reduction of nitrate to nitrite are supplied by the [4Fe-4S] cluster, which is located 12 Å from the molybdenum atom. The [4Fe-4S] cluster is the direct electron acceptor of NapB and is located near the periphery of the *Desulfovibrio* enzyme in a crevice which is lined by mainly hydrophobic residues and by a few charged residues (Arg14, His41, Lys49, Glu179, His181, Arg186, and Asp620) that may be important in mediating the interaction with NapB. Surface maps of the electrostatic potential of NapB did not reveal any reasonable interaction sites.

In fact, it appears that NapB and the NapA homologue are complementary in terms of shape. Due to the incomplete NapB structure and the use of a structural homologue of NapA, manual docking between these proteins by maximizing the contact area results in a number of plausible, although highly speculative, models, one in which the closest distance between heme I of NapB and the [4Fe-4S] cluster of NapA is only 8.7 Å (Figure 5). This short distance lies within the 14 Å range that allows high electron transfer rates and directional specificity (*23*). Several other models seem equally possible, and can be divided according to which heme is positioned closest to NapA. However, since both hemes are related by a 2-fold axis, all models result in a similar organization of the redox cofactors.

The four redox centers in the proposed NapAB complex could therefore span approximately 40 Å and are most likely positioned in a nearly linear configuration. This so-called "molecular wire" formed by a chain of multiple redox centers is also present in single redox proteins containing multiple redox centers. Examples are the soluble fumarate reductase of *Shewanella* spp., where four heme *c* groups and one FAD also span a distance of 40 Å (*49*−*51*). The cofactors of the

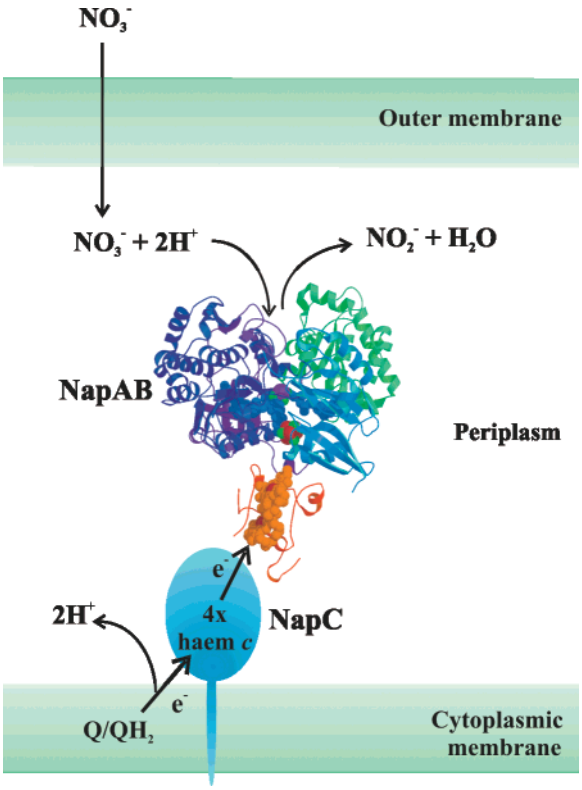

FIGURE 6: Model of the electron transfer from the quinol pool (Q/QH_2) in the cytoplasmic membrane via NapC and NapB, and ultimately to the catalytic site of NapA where nitrate is reduced to nitrite.

membrane-bound fumarate reductase of *Wolinella succinogenes* are also arranged in a linear manner, from two heme *b* groups via three different Fe−S clusters to the active site FAD (*52*). A chain of redox centers is also found in the cytochrome bc_1 complex, containing two *b*-type heme groups, one c_1-type heme, and a [2Fe-2S] center (*53*), and in flavocytochrome *c* sulfide dehydrogenase, which contains a FAD cofactor and two heme *c* groups (*28*).

In conclusion, we here present a model (Figure 6) of the Nap system whereby electrons are transferred from the tetraheme cytochrome *c* NapC to NapB and, subsequently, are conducted along the proposed 40 Å molecular wire to the nitrate molecule that has reached the catalytic site of the NapA protein through the funnel-like cavity of the latter.

ACKNOWLEDGMENT

We thank the synchrotron facilities DORIS (HASYLAB, DESY) and ESRF. A. Perrakis is acknowledged for his help in data collection at ESRF.

REFERENCES

1. Richardson, D. J., Berks, B. C., Russell, D. A., Spiro, S., and Taylor, C. J. (2001) *Cell. Mol. Life Sci. 58*, 165−178.
2. Richardson, D. J., McEwan, A. G., Page, M. D., Jackson, J. B., and Ferguson, S. J. (1990) *Eur. J. Biochem. 194*, 263−270.
3. Berks, B. C., Ferguson, S. J., Moir, J. W. B., and Richardson, D. J. (1995) *Biochim. Biophys. Acta 1232*, 97−173.
4. Reyes, F., Roldán, M. D., Klipp, W., Castillo, F., and Moreno-Vivián, C. (1996) *Mol. Microbiol. 19*, 1307−1318.
5. Reyes, F., Gavira, M., Castillo, F., and Moreno-Vivián, C. (1998) *Biochem. J. 331*, 897−904.
6. Potter, L. C., and Cole, J. (1999) *Biochem. J. 344*, 69−76.
7. Roldán, M. D., Reyes, F., Moreno-Vivián, C., and Castillo, F. (1994) *Curr. Microbiol. 29*, 241−245.
8. Richardson, D. J., and Ferguson, S. J. (1992) *Arch. Microbiol. 157*, 535−537.
9. Bell, L. C., Richardson, D. J., and Ferguson, S. J. (1990) *FEBS Lett. 265*, 85−87.
10. Carter, J. P., Hsiao, Y. H., Spiro, S., and Richardson, D. J. (1995) *Appl. Environ. Microbiol. 61*, 2852−2858.
11. Sabaty, M., Gagnon, J., and Verméglio, A. (1994) *Arch. Microbiol. 162*, 335−343.
12. Siddiqui, R. A., Warnecke-Eberz, U., Hengsberger, A., Schneider, B., Kostka, S., and Friedrich, B. (1993) *J. Bacteriol. 175*, 5867−5876.
13. Potter, L. C., Millington, P., Griffiths, L., Thomas, G. H., and Cole, J. A. (1999) *Biochem. J. 344*, 77−84.
14. Brigé, A., Cole, J. A., Hagen, W. R., Guisez, Y., and Van Beeumen, J. J. (2001) *Biochem. J. 356*, 851−858.
15. May, B. J., Zhang, Q., Li, L. L., Paustian, M. L., Whittam, T. S., and Kapur, V. (2001) *Proc. Natl. Acad. Sci. U.S.A. 98*, 3460−3465.
16. Heidelberg, J. F., Eisen, J. A., Nelson, W. C., Clayton, R. A., Gwinn, M. L., Dodson, R. J., Haft, D. H., Hickey, E. K., Peterson, J. D., Umayam, L., Gill, S. R., Nelson, K. E., Read, T. D., Tettelin, H., Richardson, D., Ermolaeva, M. D., Vamathevan, J., Bass, S., Qin, H., Dragoi, I., Sellers, P., McDonald, L., Utterback, T., Fleishmann, R. D., Nierman, W. C., and White, O. (2000) *Nature 406*, 477−483.
17. Parkhill, J., Wren, B. W., Mungall, K., Ketley, J. M., Churcher, C., Basham, D., Chillingworth, T., Davies, R. M., Feltwell, T., Holroyd, S., Jagels, K., Karlyshev, A. V., Moule, S., Pallen, M. J., Penn, C. W., Quail, M. A., Rajandream, M. A., Rutherford, K. M., van Vliet, A. H., Whitehead, S., and Barrell, B. G. (2000) *Nature 403*, 665−668.
18. Roldán, M. D., Sears, H. J., Cheesman, M. R., Ferguson, S. J., Thomson, A. J., Berks, B. C., and Richardson, D. J. (1998) *J. Biol. Chem. 273*, 28785−28790.
19. Butler, C. S., Charnock, J. M., Garner, C. D., Thomson, A. J., Ferguson, S. J., Berks, B. C., and Richardson, D. J. (2000) *Biochem. J. 352*, 859−864.
20. Butler, C. S., Charnock, J. M., Bennett, B., Sears, H. J., Reilly, A. J., Ferguson, S. J., Garner, C. D., Lowe, D. J., Thomson, A. J., Berks, B. C., and Richardson, D. J. (1999) *Biochemistry 38*, 9000−9012.
21. Butler, C. S., Ferguson, S. J., Berks, B. C., Thomson, A. J., Cheesman, M. R., and Richardson, D. J. (2001) *FEBS Lett. 500*, 71−74.
22. Dias, J. M., Than, M. E., Humm, A., Huber, R., Bourenkov, G. P., Bartunik, H. D., Bursakov, S., Calvete, J., Caldeira, J., Carneiro, C., Moura, J. J., Moura, I., and Romão, M. J. (1999) *Structure 7*, 65−79.
23. Page, C. C., Moser, C. C., Chen, X., and Dutton, P. L. (1999) *Nature 402*, 47−52.
24. Berks, B. C., Richardson, D. J., Reilly, A., Willis, A. C., and Ferguson, S. J. (1995) *Biochem. J. 309*, 983−992.
25. Fleischmann, R. D., Adams, M. D., White, O., Clayton, R. A., Kirkness, E. F., Kerlavage, A. R., Bult, C. J., Tomb, J., Dougherty, B. A., Merrick, J. M., McKenney, K., Sutton, G., FitzHugh, W., Fields, C., Gocayne, J. D., Scott, J., Shirley, R., Liu, L., Glodek, A., Kelley, J. M., Weidman, J. F., Phillips, C. A., Spriggs, T., Hedblom, E., Cotton, M. D., Utterback, T. R., Hanna, M. C., Nguyen, D. T., Saudek, D. M., Brandon, R. C., Fine, L. D., Fritchman, J. L., Fuhrmann, J. L., Geoghagen, N. S. M., Gnehm, C. L., McDonald, L. A., Small, K. V., Fraser, C. M., Smith, H. O., and Venter, J. C (1995) *Science 269*, 496−512.
26. Richterich, P., Lakey, N., Gryan, G., Jaehn, L., Mintz, L., Robison, K., and Church, G. M. (1993) Unpublished DNA sequence in the EMBL/GenBank/DDBJ Nucleotide Sequence Data Library under Accession Number U00008.
27. Kadziola, A., and Larsen, S. (1997) *Structure 15*, 203−216.
28. Chen, Z.-W., Koh, M., Van Driessche, G., Van Beeumen, J., Bartsch, R. G., Meyer, T. E., and Mathews, F. S. (1994) *Science 266*, 430−432.

29. Fülöp, V., Ridout, C. J., Greenwood, C., and Hajdu, J. (1995) *Structure 3*, 1225−1233.
30. Matias, P. M., Morais, J., Coelho, A. V., Meijers, R., Gonzalez, A., Thompson, A. W., Sieker, L., LeGall, J., and Carrondo, M. A. (1997) *J. Biol. Inorg. Chem. 2*, 507−514.
31. Brigé, A., Leys, D., and Van Beeumen, J. J. (2001) *Acta Crystallogr. D57*, 418−420.
32. Mathews, B. W. (1968) *J. Mol. Biol. 33*, 491−497.
33. Perrakis, A., Cipriani, F., Castagna, J.-C., Claustre, L., Burghammer, M., Riekel, C., and Cusack, S. (1999) *Acta Crystallogr. D55*, 1765−1770.
34. Otwinowski, Z., and Minor, W. (1997) *Methods Enzymol. 276*, 307−326.
35. Collaborative Computational Project Number 4 (1994) *Acta Crystallogr. D50*, 760−763.
36. Otwinowski, Z. (1991) in *Isomorphous replacement and anomalous scattering*, Vol. 80, SERC Daresbury Laboratory, Warrington, England.
37. Roussel, A., and Cambillau, C. (1992) *TURBO-FRODO*, Biographics, AFMB, Marseille, France.
38. Perrakis, A., Morris, R., and Lamzin, V. S. (1999) *Nat. Struct. Biol. 6*, 458−463.
39. Murshudov, G. N., Vagin, A. A., and Dodson, E. J. (1997) *Acta Crystallogr. D53*, 240−255.
40. Sheldrick, G. M., and Schneider, T. R. (1997) *Methods Enzymol. 277*, 319−343.
41. Holm, L., and Sander, C. (1993) *J. Mol. Biol. 233*, 123−138.
42. Kraulis, P. J. (1991) *J. Appl. Crystallogr. 24*, 946−950.
43. Merrit, E. A., and Murphy, M. E. P. (1994) *Acta Crystallogr. D50*, 869−873.
44. Kostanjevečki, V., Leys, D., Van Driessche, G., Meyer, T. E., Cusanovich, M. A., Fischer, U., Guisez, Y., and Van Beeumen, J. J. (1999) *J. Biol. Chem. 274*, 35614−35620.
45. Igarashi, N., Moriyama, H., Fujiwara, T., Fukumori, Y., and Tanaka, N. (1997) *Nat. Struct. Biol. 4*, 276−284.
46. Sayle, R. A., and Milner-White, E. J. (1995) *Trends Biochem. Sci. 20*, 374.
47. Iverson, T. M., Arciero, D. M., Hsu, B. T., Logan, M. S. P., Hooper, A. B., and Rees, D. C. (1998) *Nat. Struct. Biol. 5*, 1005−1012.
48. Einsle, O., Messerschmidt, A., Stach, P., Bourenkov, G. P., Bartunik, H. D., Huber, R., and Kroneck, P. M. H. (1999) *Nature 400*, 476−480.
49. Bamford, V., Dobbin, P. S., Richardson, D. J., and Hemmings, A. M. (1999) *Nat. Struct. Biol. 6*, 1104−1107.
50. Taylor, P., Pealing, S. L., Reid, G. A., Chapman, S. K., and Walkinshaw, M. D. (1999) *Nat. Struct. Biol. 6*, 1108−1112.
51. Leys, D., Tsapin, A. S., Nealson, K. H., Meyer, T. E., Cusanovich, M. A., and Van Beeumen, J. J. (1999) *Nat. Struct. Biol. 6*, 1113−1117.
52. Lancaster, C. R., Kroger, A., Auer, M., and Michel, H. (1999) *Nature 402*, 377−385.
53. Iwata, S., Lee, J. W., Okada, K., Lee, J. K., Iwata, M., Rasmussen, B., Link, T. A., Ramaswamy, S., and Jap, B. K. (1998) *Science 281*, 64−71.

BI012144B